Application of PS-wave moveout asymmetry in parameter estimation for tilted TI media – Part II: Dipping TTI layer

Pawan Dewangan[†] and Ilya Tsvankin[†]
[†] *Center for Wave Phenomena, Department of Geophysics, Colorado School of Mines, Golden, CO 80401-1887*

ABSTRACT
Dipping transversely isotropic layers with a tilted symmetry axis (TTI media) cause serious imaging problems in fold-and-thrust belts and near salt domes. Here, we apply the modified PP+PS=SS method introduced in Part I to the inversion of long-spread PP and PS reflection data for the parameters of a TTI layer with the symmetry axis orthogonal to the bedding. The inversion algorithm combines the asymmetry attributes of the PSV-wave with the hyperbolic moveout of the pure PP- and SS-waves in the symmetry-axis plane (i.e., the vertical plane that contains the symmetry axis).
Analysis of the asymmetry attributes for a dipping layer is complicated by the fact that the PS-waves with the same conversion point do not have identical ray parameters (horizontal slownesses). The weak-anisotropy, small-offset approximations for the time and offset asymmetry factors show that the leading terms in offset do not contain independent information for the inversion. Therefore, the parameter-estimation algorithm has to rely on long-offset PS data (with maximum offset-to-depth ratios of at least two), which makes the results generally less stable than those for a horizontal TTI layer in Part I.
Still, the contribution of the PS-wave asymmetry factors helps to constrain the TTI parameters for large tilts ν of the symmetry axis ($\nu > 40^\circ$). The least resolved parameter is Thomsen's coefficient ϵ because it that does not directly influence the moveout signatures of either pure or converted modes. The accuracy in ϵ and other parameters for large tilts can be improved by using wide-azimuth PP and PS reflections. With high-quality PS data, the inversion remains feasible for moderate tilts ($25^\circ < \nu < 40^\circ$), but it breaks down for models with smaller values of ν in which the moveout asymmetry is too weak. However, the tilt itself and several combinations of the medium parameters (e.g., the ratio of the symmetry-direction P-and S-wave velocities and the anisotropic parameter χ) are well-constrained for all symmetry-axis orientations.
The inversion results prove that 2D measurements of the PS-wave asymmetry attributes can be effectively used in velocity analysis for dipping TTI layers. In addition to providing an improved velocity model for imaging beneath TTI beds, our algorithm can yield valuable information for lithology discrimination and structural interpretation.

Key words: converted waves, dipping shale, moveout asymmetry

1 INTRODUCTION

Estimation of the parameters of tilted transversely isotropic (TTI) media is essential for anisotropic imaging beneath TTI formations and characterization of dipping fracture systems. Mode-converted PS-waves can make an important contribution to building TTI ve-

locity models because of their high sensitivity to the anisotropic parameters.

In our previous paper on this topic (Dewangan and Tsvankin, 2003; hereafter referred to as Paper I), we proposed a modification of the PP+PS=SS method developed by Grechka and Tsvankin (2002) and Grechka and Dewangan (2003) for joint processing of PP and PS reflection data. In addition to the "quasi-shear" waves that possess the kinematics of pure SS primaries, our algorithm generates attributes of the moveout asymmetry of PS-waves. We also showed that the asymmetry attributes provide crucial information needed to estimate the parameters of a horizontal TTI layer from surface PP and PS data.

The moveout of PS-waves becomes asymmetric if the traveltime does not remain the same when the source and receiver are interchanged. In the case of a horizontal TTI layer, the asymmetry is caused by the tilt of the symmetry axis which may be associated, for example, with a set of dipping penny-shaped cracks (Paper I). Another possible reason for the PS-wave moveout asymmetry is lateral heterogeneity in the form of lateral velocity variations or non-horizontal reflectors. For example, PS moveout becomes asymmetric even in an isotropic or VTI (TI with a vertical symmetry axis) layer above a plane dipping reflector (Tsvankin and Grechka, 2000).

In active tectonic areas, originally horizontal TI layers are often rotated in such a way that the symmetry axis remains orthogonal to the layer boundaries. Dipping shale layers of this type are commonly observed in the fold-and-thrust region of the Canadian Foothills (e.g., Isaac and Lawton, 1999) and near salt domes. Ignoring anisotropy in dipping TTI beds causes significant mispositioning of reflection events in both vertical and horizontal directions (Issac and Lawton, 1999; Vestrum et al., 1999; Lawton et. al., 2001). Although migration algorithms can be readily extended to TTI media, accurate estimation of the anisotropic parameters for imaging purposes remains a difficult problem.

2D inversion of P-wave normal-moveout (NMO) velocities for the parameters of dipping TTI layers with the symmetry axis perpendicular to the bedding was discussed by Grechka et al. (2001). Although their method performed well on physical-modeling data, it is based on a number of simplifying assumptions about the model (e.g., the medium around the TTI layer has to be isotropic and homogeneous). Also, in addition to reflections from the TTI layer itself, the algorithm of Grechka et al. (2001) requires reflection data from a deeper horizontal interface. A review of several other velocity-analysis algorithms for TTI media (Grechka and Tsvankin, 2000; Grechka et al., 2002) can be found in Paper I. It should be emphasized that none of the existing methods can yield stable parameter estimates for moderate dips or tilts of the symmetry axis (up to 40°) using reflections from the bottom of the TTI layer, even if multicomponent, wide-azimuth data are available. The parameter estimation for mild dips (15-20° or larger), however, was shown to be feasible for a TI layer with a vertical symmetry axis (VTI), if the asymmetry attributes of the PSV-wave are included in the inversion (Tsvankin and Grechka, 2000; 2002).

Here, we extend the methodology introduced in Paper I to the inversion of multicomponent (PP and PSV) data acquired above a TTI layer with the symmetry axis orthogonal to the layer's bottom. The moveout asymmetry of PS-waves in this model is caused by both the reflector dip ϕ and the tilt ν of the symmetry axis, which are assumed to be equal to each other. The modified PP+PS=SS method yields the PSV-wave asymmetry attributes, which we combine in the inversion procedure with the NMO velocities, zero-offset traveltimes and reflection slopes of the pure PP and SS reflections.

The inversion algorithm is designed to estimate the P- and S-wave velocities in the symmetry direction (V_{P0} and V_{S0}, respectively), Thomsen (1986) anisotropic parameters ϵ and δ, the tilt ν and the thickness of the layer using solely reflection traveltimes. We present simple analytic approximations for the time and offset asymmetry factors of the PSV-wave and demonstrate that independent information for the inversion is contained in higher-order terms in offset that become substantial as the offset-to-depth ratio approaches two. Numerical tests for variable errors in the asymmetry attributes help to evaluate the resolution in each parameter for a wide range of plausible TTI models.

2 ASYMMETRIC PS-WAVE MOVEOUT IN A DIPPING TTI LAYER

2.1 Moveout asymmetry from the PP+PS=SS method

For laterally heterogeneous models, such as a layer above a dipping reflector, the moveout of converted waves becomes asymmetric even in the absence of anisotropy (e.g., Tsvankin and Grechka, 2000). This asymmetry is commonly observed on split-spread CMP gathers in the offset domain because the traveltime does not stay the same when the source and receiver positions are interchanged. However, since these "reciprocal" traveltimes correspond to different conversion points, offset-domain measurements of the moveout asymmetry may be distorted by the influence of the reflector shape.

An important advantage of estimating the asymmetry from the PP+PS=SS method is that each pair of the reciprocal PS events is guaranteed to have the same conversion point. Indeed, the method is designed to identify two PS-waves converted at the reflection point of a given PP-arrival (see Figure 1 in Paper I). Then the traveltime of the SS-wave, which is not physically excited by the source, is obtained by combining the reflection times of the PP-wave and two PS-waves.

We consider a homogeneous TTI layer with the axis of symmetry orthogonal to the layer's bottom (reflector) that may have an arbitrary dip. Hence, the symmetry axis is confined to the reflector's dip plane that represents the only vertical symmetry plane of the model (we call it the symmetry-axis plane). The x_1-axis of the Cartesian coordinate system points in the updip direction of the reflector (Figure A1).

According to Snell's law, the projection of the slowness vector onto the reflector should be the same for all reflected waves. If we denote the slowness components in the dip and strike directions of the reflector by $p_{\rm int1}$ and $p_{\rm int2}$ (both $p_{\rm int1}$ and $p_{\rm int2}$ are confined to the reflector plane), the difference between the traveltimes of the two PS-waves with the same conversion point can be represented as

$$\begin{aligned}\Delta t_{PS} &= t_{PS}(p_{\rm int1}, p_{\rm int2}) - t_{PS}(-p_{\rm int1}, -p_{\rm int2}) \qquad (1)\\ &= \Delta t_P + \Delta t_S,\end{aligned}$$

where Δt_P and Δt_S are the contributions to Δt_{PS} from the P- and S-legs of the PS ray, respectively. Equation (1) has the same form as the expression for Δt_{PS} in Paper I, where the slowness components have to be computed for a *horizontal* interface.

Following Paper I, we also define the measure of asymmetry in the offset $\boldsymbol{x}$ [equation (A4)] using the two PS-waves with the opposite signs of the slowness projection onto the reflector:

$$\boldsymbol{\Delta x}_{PS} = \boldsymbol{x}_{PS}(p_{\rm int1}, p_{\rm int2}) + \boldsymbol{x}_{PS}(-p_{\rm int1}, -p_{\rm int2}). \qquad (2)$$

To gain insight into the influence of the model parameters on the time and offset asymmetry factors, we analyze approximate expressions for Δt_{PS} and $\boldsymbol{\Delta x}_{PS}$ obtained in Appendices A and B under the assumption of weak anisotropy ($|\epsilon| \ll 1$ and $|\delta| \ll 1$) and small offset-to-depth ratio ($|p_{\rm int1} V_{P0}| \ll 1$ and $|p_{\rm int2} V_{P0}| \ll 1$). As shown in Appendix A, the approximate moveout asymmetry factor Δt_{PS} for the PSV-wave in the symmetry-axis plane (i.e., for the azimuth $\alpha = 0$) is given by

$$\begin{aligned}\Delta t_{PS} &= \frac{-2\sin\nu}{V_{S0}}\,\chi\, x_{SS} \qquad (3)\\ &+ \frac{(1+4\epsilon)\,V_{P0}^2\,\sin\nu\cos^2\nu}{4\,(1+2\sigma)^3\,V_{S0}^3\,z_d^2}\; x_{SS}^3,\end{aligned}$$

where $\chi \equiv (\sigma-\delta)/(1+2\sigma)$ is the anisotropic parameter that can be obtained from the zero-offset traveltimes and NMO velocities of P- and SV-waves in layer-cake VTI media (Grechka and Dewangan, 2003), and z_d is the normal distance from the common midpoint (CMP) to the reflector. As expected, the asymmetry factor Δt_{PS} vanishes for zero tilt and dip ($\nu = 0$) when the medium becomes VTI. The linear term in offset is proportional to the anisotropic parameter χ that can be estimated from the moveout of pure PP and SS reflections (see below), so it does not carry independent information for velocity analysis. Note that PS moveout is asymmetric even in a dipping isotropic layer, where the cubic [equation (3)] and higher-order terms in x_{SS} do not go to zero. Figure 1 shows the asymmetry factor Δt_{PS} computed for a typical dipping TTI model from the exact equations (1) and (A1), as well as from approximation (3). While the initial slope of Δt_{PS} is well-described by the linear term in equation (3), the cubic and higher-order terms make a significant contribution at far offsets that correspond to offset-to-depth ratios of about two for the original PP and PS data. The linear term provides a good approximation for Δt_{PS} at near offsets even for larger absolute values of δ and σ when equation (3) as a whole becomes inaccurate.

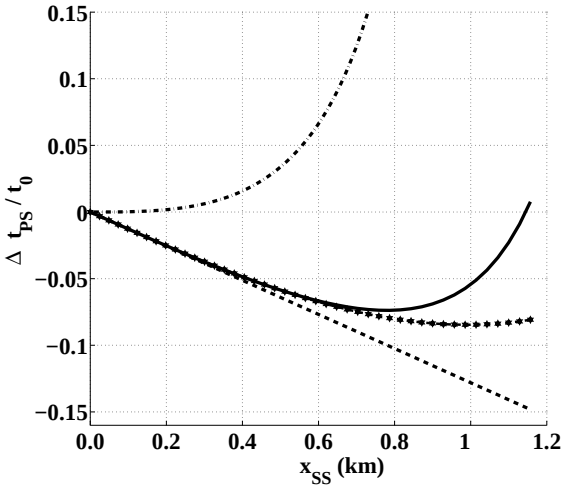

Figure 1. Time asymmetry factor Δt_{PS} for the PSV-wave in the symmetry-axis plane of a dipping TTI layer. The exact asymmetry factor is marked by the solid line, the weak-anisotropy approximation (3) by the dashed line with stars, the linear term in equation (3) by the dashed line, and Δt_{PS} in the reference isotropic model by the dash-dotted line. Δt_{PS} is normalized by the zero-offset traveltime of the PS-wave. The medium parameters are $V_{P0} = 4$ km/s, $V_{S0} = 2$ km/s, $\epsilon = 0.25$, $\delta = 0.1$, $\nu = 25°$, and $z_d = 1$ km. The maximum offset-to-depth ratio of the PP and PS data is close to two.

The weak-anisotropy approximation for the azimuthally varying offset asymmetry factor [equation (2)] is derived in Appendix B. In the symmetry-axis plane ($\alpha = 0$), the approximate Δx_{PS} takes the following form:

$$\Delta x_{PS} = \frac{\sin\nu}{2\,z_d}\left[\frac{(1+4\delta)\,V_{P0}^2}{(1+4\sigma)\,V_{S0}^2} - 1\right] x_{SS}^2. \qquad (4)$$

Equation (4) indicates that for typical TI models with $\sigma \gg \delta$, the influence of anisotropy *reduces* the offset asymmetry factor, which is confirmed by the numerical results in Figure 2. The weak-anisotropy approximation (4) deteriorates with increasing offset because the exact solution is influenced by the quartic term in x_{SS} even for offset-to-depth ratios of the PS-wave close to two. For the moderately anisotropic model in Fig-

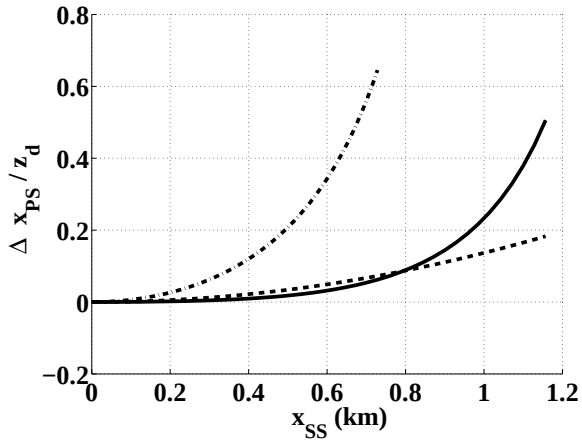

Figure 2. Offset asymmetry factor Δx_{PS} for the PSV-wave in the symmetry-axis plane. The exact Δx_{PS} is marked by the solid line, the weak-anisotropy approximation (4) by the dashed line, and Δx_{PS} in the reference isotropic model by the dash-dotted line. The factor Δx_{PS} is normalized by the distance z_d between the CMP and the reflector. The medium parameters are the same as those in Figure 1.

ure 2, the magnitude of the factor Δx_{PS} reaches up to 50% of the CMP–reflector distance. However, as discussed below, the leading (x_{SS}^2) term in equation (4) does not contain independent information for estimating the model parameters.

For a dipping layer, the minimum traveltime of PS-wave on a CMP gather is not recorded at zero offset. An analytic expression for the azimuthally dependent offset $x_{\min}(\alpha)$ of the traveltime minimum is obtained in Appendix B by assuming a small dip ν and linearizing the exact equation in the anisotropic parameters. In the symmetry-axis plane, the approximation for $x_{\min}$ reduces to

$$x_{\min}(\alpha = 0) = \frac{z_d}{2\cos^2\nu}\left[\frac{\sin\nu}{V_{P0}} - \frac{\sin\nu}{V_{S0}}\right] \left[V_{P0}(1+2\delta) + V_{S0}(1+2\sigma)\right]. \quad (5)$$

Although anisotropy does make a substantial contribution to $x_{\min}(\alpha = 0)$, all terms in equation (5) can be found from the NMO velocities, zero-offset traveltimes and reflection slopes of the pure (PP and SS) reflection modes (see below).

3 PARAMETER ESTIMATION IN A TTI LAYER

3.1 Data processing

The main prerequisite for successful application of the inversion algorithm discussed here is acquisition of long-offset PP and PS data (Grechka and Tsvankin, 2002; Paper I). First, offset-to-depth ratios of at least two for the recorded PP- and PS-waves are needed for stable estimation of the NMO velocity of the constructed SS arrivals. Second, acquiring PS data for a wide range of offsets ensures a sufficiently large magnitude of the moveout asymmetry attributes used in the parameter estimation.

The data processing flow is similar to that described in Paper I. The PP+PS=SS method yields "quasi-shear" data, whose reflection moveout can be used to estimate the stacking (NMO) velocity ($V_{\rm nmo,S}$), zero-offset traveltime (t_{S0}) and time slopes on zero-offset section (i.e., the ray parameter p_{S0}) for the SS-waves. The same parameters for the recorded PP-waves ($V_{\rm nmo,P}$, t_{P0}, and p_{P0}) can be obtained from conventional hyperbolic semblance analysis. For wide-azimuth data, the NMO velocities of the PP- and SS-waves are replaced by the NMO ellipses determined from azimuthal moveout analysis (Grechka and Tsvankin, 1999; Paper I). As described in Paper I, we combine the moveout parameters of the pure PP ad SS reflections with the two PS-wave asymmetry attributes obtained from a modified PP+PS=SS method: Δt_{PS} [equations (1) and (3)] and Δx_{PS} [equations (2) and (4)]. The offset $x_{\min}$ [equation (5)] does not contain any additional information about the model and, therefore, is not included in the inversion.

3.2 Inversion algorithm

Suppose that both PP and PS (PSV) reflection data are acquired in a 3D survey for a wide range of azimuths, and the PP+PS=SS method is used to generate quasi-S reflections and the asymmetry attributes of the PSV-wave. Then the orientation of the symmetry-axis plane can be established from the NMO ellipses of the pure modes, whose axes are aligned with the dip and strike directions of the reflector. Processing of the PP-waves yields the semi-axes of the P-wave NMO ellipse ($V_{\rm nmo,P}^{\rm dip}$ and $V_{\rm nmo,P}^{\rm strike}$), the zero-offset traveltime, and the time slope on the zero-offset section:

$$V_{\rm nmo,P}^{\rm dip} = \frac{V_{P0}\sqrt{1+2\delta}}{\cos\nu}, \quad V_{\rm nmo,P}^{\rm strike} = V_{P0}\sqrt{1+2\delta}, \quad (6)$$

$$t_{P0} = \frac{z_d}{V_{P0}}, \quad (7)$$

$$p_{P0} = \frac{\sin\nu}{V_{P0}}. \quad (8)$$

The velocity $V_{\rm nmo,P}^{\rm dip}$ for the TTI model with the symmetry axis orthogonal to the reflector is derived in Tsvankin (1995, 2001); the strike component of the NMO ellipse can be found in a similar way. The expressions for t_{P0} and p_{P0} are obtained using the fact that the zero-offset ray in our model travels along the symmetry axis. The corresponding attributes for the SS-wave can be estimated from the quasi-S data:

$$V_{\rm nmo,S}^{\rm dip} = \frac{V_{S0}\sqrt{1+2\sigma}}{\cos\nu}, \quad V_{\rm nmo,S}^{\rm strike} = V_{S0}\sqrt{1+2\sigma}, \quad (9)$$

$$t_{S0} = \frac{z_d}{V_{S0}}, \tag{10}$$

$$p_{S0} = \frac{\sin\nu}{V_{S0}}. \tag{11}$$

The model vector for the TTI layer includes the following components:

$$\boldsymbol{m} \equiv \left\{ V_{P0}\,,\; V_{S0}\,,\; \epsilon\,,\; \delta\,,\; \nu=\phi,\; z_d \right\}, \tag{12}$$

where the tilt ν of the symmetry axis is taken to be equal to the reflector dip ϕ. For noise-free data, all six model parameters can be recovered uniquely using the NMO velocities, zero-offset traveltimes and zero-offset slopes of the PP- and SS-waves. Indeed, the tilt ν can be found from the ratio of the NMO velocities of either wave in the dip and strike directions, which allows us to obtain the vertical velocities V_{P0} and V_{S0} from the ray parameters p_{P0} and p_{S0}. Finally, the distance z_d and parameters ϵ and δ can be inferred from the zero-offset times and NMO ellipses. However, in the presence of noise, the estimation of tilt from the ratio of the NMO velocities is highly unstable for small and moderate tilts.

This instability can be illustrated by computing the range of possible tilt values for the NMO velocities contaminated by Gaussian noise with a standard deviation of 2% (Figure 3). Although the estimation of tilt is unbiased, with the distribution centered at the correct value ($\nu = 25°$), the standard deviation of ν is about 3.5°. According to the sensitivity plots in Figure 4, such a scatter in ν is sufficient to cause unacceptably large errors in the parameters ϵ and V_{P0} reaching 0.3 and 15%, respectively. Thus, a realistic distortion of 1–2% in the NMO velocities propagates with a significant amplification into the other parameters. This conclusion is also supported by the results of Grechka et al. (2002) who found the inversion of the PP and SS (SVSV) NMO ellipses, zero-offset times and reflection slopes in a dipping TTI layer to be nonunique for tilts and dips smaller than 30–40°.

It is equally important for practical applications to study the inverse problem for the common case when only 2D data in the symmetry-axis plane are available. The data vector in this case has six elements ($V^{\rm dip}_{\rm nmo,P}$, t_{P0}, p_{P0}, $V^{\rm dip}_{\rm nmo,S}$, t_{S0}, and p_{S0}) but only five of them are independent because of the constraint,

$$\frac{p_{S0}}{p_{P0}} = \frac{t_{S0}}{t_{P0}}. \tag{13}$$

Since the model vector (12) includes six parameters, 2D inversion cannot be carried out without additional information, such as the asymmetry attributes of the PS-wave. The results of the previous section, however, indicate that the leading terms in the expressions for asymmetry attributes depend just on the moveout parameters of the pure (PP and SS) modes. Indeed, rewriting equations (3), (4), and (5) in terms of NMO velocities, zero-offset times and reflection slopes of the PP- and SS-waves, we find [only the linear term in equation (3) is included]

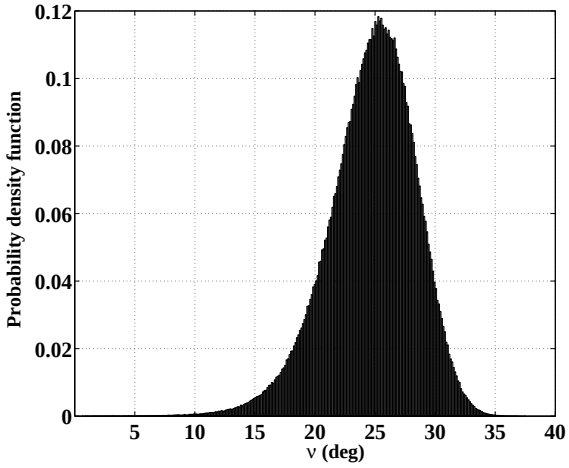

Figure 3. Probability density function of the tilt ν assuming a 2% error in the NMO velocities. The model parameters are the same as those in Figure 1.

$$\Delta t_{PS} = p_{S0}\left(\frac{V^2_{\rm nmo,P}\,t^2_{P0}}{V^2_{\rm nmo,S}\,t^2_{S0}} - 1\right) x_{SS}\,, \tag{14}$$

$$\Delta x_{PS} = \frac{p_{S0}}{2\,t_{S0}}\left(\frac{V^4_{\rm nmo,P}\,t^2_{P0}}{V^4_{\rm nmo,S}\,t^2_{S0}} - 1\right) x^2_{SS}\,, \tag{15}$$

$$x_{\rm min} = \frac{t_{S0}}{2p_{S0}}\left(p_{P0} - p_{S0}\right) \left(V^2_{\rm nmo,P}\,p_{P0} + V^2_{\rm nmo,S}\,p_{S0}\right). \tag{16}$$

All NMO velocities in equations (14)–(16) are the dip components of the NMO ellipses measured in the symmetry-axis plane.

Clearly, only the *deviations* of the exact asymmetry attributes from the approximations (14)–(16) can provide independent information for the parameter estimation. As illustrated by Figures 1 and 2, such deviations do become substantial at large offsets x_{SS} for both the time and offset asymmetry factors.

We propose the following algorithm to invert the 2D multicomponent data in the symmetry-axis plane for the model vector (12):

- For each value of the tilt ν from 0° to 90°, find the model vector using equations (6)–(11). Restrict the range of plausible tilts by putting reasonable constraints on the parameter ϵ ($0 \le \epsilon \le 1$; see Figure 4 below).
- Taking into account errors in the measured quantities, compute the range of models that fit the data within the noise level for each plausible tilt.
- For each model found in the previous step, compute the asymmetry attributes from the exact equations (1) and (2).
- Calculate the following misfit function for the asymmetry attributes over the full range of offsets (the maximum offset-to-depth ratio of the PP and PS data

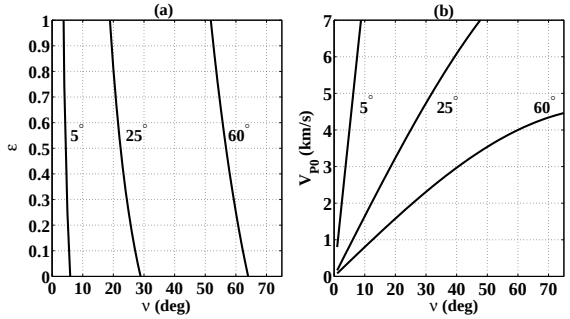

Figure 4. Range of possible solutions for the parameters ϵ (a) and V_{P0} (b) for three values of the tilt: $\nu = 5°$, $25°$ and $60°$. All model parameters except for ν are the same as those in Figure 1 ($\epsilon = 0.25$, $V_{P0} = 4$ km/s).

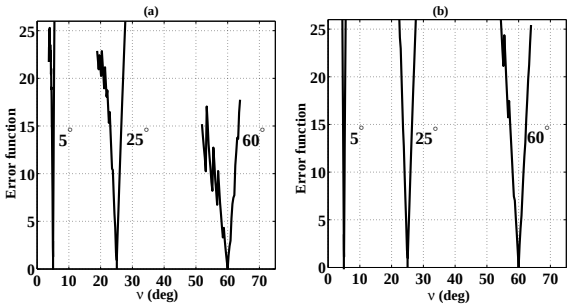

Figure 5. Square-root of the misfit function (17) for (a) the time asymmetry factor Δt_{PS}; and (b) the offset asymmetry factor Δx_{PS}. The misfit function is computed for the models in Figure 4 which fit the pure-mode data and satisfy the constraint $0 \le \epsilon \le 1$.

should be no smaller than two):

$$\mathcal{F} \equiv \frac{\sum(\Delta t_{PS}^{\rm calc} - \Delta t_{PS}^{\rm meas})^2}{(\sum \Delta t_{PS}^{\rm meas})^2} + \frac{\sum (\Delta x_{PS}^{\rm calc} - \Delta x_{PS}^{\rm meas})^2}{(\sum \Delta x_{PS}^{\rm meas})^2} . \quad (17)$$

- Identify the model vector that minimizes this misfit function.

Prior to applying the inversion algorithm, we present the sensitivity analysis for noise-free data. For the test in Figure 4, we computed the NMO velocities, zero-offset traveltimes and zero-offset slopes for the PP- and SS-waves from the exact equations for three different values of the tilt ν. Then, for each of the three models we scanned over tilt and computed the model parameters from equations (6)–(11), as described above. It is clear from Figure 4a that the parameter ϵ is highly sensitive to ν, and only a narrow range of tilts produces plausible ϵ values within the interval $0 \le \epsilon \le 1$. The variation of ϵ with ν is particularly rapid for small tilts corresponding to models approaching VTI. Therefore, putting reasonable constraints on ϵ helps to substantially reduce the range of ν for which we need to compute the asymmetry attributes at the second stage of the inversion procedure.

According to Figure 4a, small errors in ν may produce large distortions in ϵ, especially for mild tilts. The problem in resolving ϵ is related to the fact that it contributes to the data vector only indirectly, through the parameter σ [equations (6)–(11)]. Both σ and δ are more tightly constrained by the input data than is ϵ (see below), with the exception of quasi-VTI models with small ν for which the inversion as a whole breaks down. In contrast to ϵ, the vertical velocity V_{P0} is much less sensitive to the tilt, especially for moderate and large values of ν (Figure 4b). The dependence of the parameters V_{S0} and z_d on ν shows a pattern similar to that for V_{P0}.

To distinguish between the models that fit the pure-mode data, we use the time and offset asymmetry factors in the symmetry-axis plane. Figure 5 displays the square-root of the objective (misfit) function (17), which is equivalent to the standard deviation of the error in each of the asymmetry attributes. The expected value of the misfit function can be represented as

$$E[\mathcal{F}] = E\left[\frac{\{x-(x+\alpha\cdot x)\}\cdot\{x-(x+\alpha\cdot x)\}}{x\cdot x}\right] = E[\alpha^2] = \sigma_\alpha^2 + (E[\alpha])^2 = \sigma_\alpha^2 ,$$

where α is a random variable with zero mean and the standard deviation σ_α, and x is the vector of either the time or offset asymmetry values for different offsets.

For noise-free data, all model parameters can be estimated uniquely because the misfit function for both Δt_{PS} and Δx_{PS} goes to zero at the correct tilt angle (Figure 5). In the presence of noise, the resolution in tilt becomes lower for larger values of ν where the misfit function increases more slowly away from the correct solution. This result is supported by equation (3) for the time asymmetry factor Δt_{PS} in which the ratio of the cubic and linear terms in offset decreases with ν. As discussed above, only the cubic and higher-order terms in the equation for Δt_{PS} contain independent information for the inversion. Note that the high resolution in ν for quasi-VTI models with mild tilt does not mean that the rest of the parameters can be estimated with high accuracy. Despite the tight constraints on the tilt provided by both the pure-mode signatures and the asymmetry attributes, not only ϵ, but also δ and the vertical velocities are too sensitive to tilt for the inversion to be sufficiently stable (see the numerical results below).

Figure 5 also shows that the time and offset asymmetry factors provide comparable resolution in tilt, although the factor Δx_{PS} performs somewhat better for relatively large tilts and also for large errors in the asymmetry factors. Therefore, the inversion algorithm employs equation (17) with equal weights for Δt_{PS} and Δx_{PS}. Typically, the misfit function based on the time asymmetry has more local minima than that based on

the offset asymmetry. The asymmetry information becomes useless for the inversion purposes if errors reach 20% in Δt_{PS} and 40% in Δx_{PS}.

3.3 Numerical examples

To evaluate the stability of the parameter estimation, we present a series of numerical tests in which the input data were computed from the exact equations for a representative range of TTI models and contaminated by Gaussian noise. For each model, the parameter vector m [equation (12)] is obtained for 200 realizations of the input data using the inversion algorithm described above.

In the previous section, we showed that the leading terms in x_{SS} in the equations for the asymmetry attributes do not provide independent information for the parameter estimation. Therefore, to assess the accuracy of the inversion, it is convenient to define the "quality factor" for the time asymmetry Δt_{PS} as

$$Q = \max\left\{\frac{|\Delta t_{PS}^{\rm lin} - \Delta t_{PS}^{\rm exact}|}{|\Delta t_{PS}^{\rm lin}|}\right\}, \qquad (18)$$

where $\Delta t_{PS}^{\rm exact}$ is the exact value and $\Delta t_{PS}^{\rm lin}$ is the linear term in x_{SS} [equation (3)]; Q is computed for the maximum offset-to-depth ratio of two for the PS-waves. Since the sensitivity of the offset asymmetry factor to the model parameters is similar to that for the time asymmetry (see Figure 5), we do not include Δx_{PS} in equation (18). If the quality factor is large (close to or greater than unity, according to our estimates), we expect the asymmetry attributes to make a substantial contribution to the inversion for the tilt ν and other parameters.

First, we consider TTI media with large tilts of the symmetry axis ($\nu > 40^\circ$), which also implies steep reflector dips. Such models are typical for the Rocky Mountain Foothills in Western Canada and other fold-and-thrust belts that contain steeply dipping TI shale layers (e.g., Isaac and Lawton, 1999). The inversion for $\nu = 60^\circ$ produces unbiased results, with the mean of each model parameter being close to the correct value (Figure 6). Although the quality factor for the model in Figure 6 is smaller than unity ($Q = 0.6$), the moveout asymmetry is quite pronounced, with the maximum of Δt_{PS} reaching 20% of the zero-offset PS traveltime, and Δx_{PS} at far offsets reaching 70% of z_d. In comparison, for the reference isotropic medium with $\epsilon = \delta = 0$, the quality factor is infinite, the maximum of Δt_{PS} is also 20% of the zero-offset time, and Δx_{PS} is up to 110% of z_d. Since the magnitude of the asymmetry attributes is relatively large, it should be possible to estimate both Δt_{PS} and Δx_{PS} with high accuracy.

If we assume that the error in the asymmetry attributes is 2%, the parameters V_{P0}, V_{S0}, and z_d are well constrained (the standard deviation is less than 1%), and the standard deviation in ν is only 1°(Figure 6). However, in agreement with the relatively small value of the quality factor, the inverted anisotropic parameters ϵ and δ exhibit more scatter, with the standard deviation reaching 0.06 and 0.04, respectively. Also, the estimates of ϵ and δ degrade rapidly as the error in the asymmetry attributes increases, while the deviations in V_{P0}, V_{S0}, and z_d remain small. It is clear from Figure 6 that the best-constrained parameter combinations are $\chi \equiv (\sigma - \delta)/(1 + 2\sigma)$, $\sin\nu/z_d$, and V_{P0}/V_{S0}. In principle, ϵ and δ for large tilts can be obtained with sufficient accuracy from wide-azimuth PP and SS data, as demonstrated by Grechka et. al. (2002).

If the tilt for the model from Figure 6 is reduced from 60° to 25° (Figure 7), the quality factor Q increases to 1.1, which indicates that for the same errors in the input data the inversion should become more stable (i.e., the model parameters should be better resolved). The magnitude of Δt_{PS} for $\nu = 25^\circ$, however, decreases to just 8% of zero-offset time (the corresponding value for the reference isotropic medium is 14%). Therefore, it is reasonable to assume that the uncertainty in the Δt_{PS} and Δx_{PS} becomes larger for mild tilts.

If the error in the asymmetry attributes is set to 6%, the standard deviation of the tilt ν is almost the same (1°) as that in Figure 6. Despite the high resolution in ν, Figure 7 shows that the standard deviations in V_{P0}, V_{S0}, and z_d increase to about 4%; the deviations in ϵ and δ are also substantial (0.08 and 0.05, respectively). Although the accuracy in all model parameters becomes acceptable if the error in the asymmetry attributes is limited to 2%, the small magnitude of Δt_{PS} and Δx_{PS} makes such low error levels unrealistic.

An interesting special case is that of an elliptically anisotropic medium ($\epsilon = \delta$). For the same tilt $\nu = 25^\circ$ as that in Figure 7, but with $\epsilon = \delta = 0.2$, the qualify factor $Q = 2.1$, which indicates significant higher-order terms in offset in the equations for Δt_{PS} and Δx_{PS}. The magnitude of the time asymmetry factor is also substantial (about 20% of zero-offset time), so the inversion is expected to be stable. It turns out, however, that the parameter estimation is feasible only if the elliptical condition is assumed in advance (i.e., the inversion is performed with $\epsilon = \delta$). If the inversion is carried out without any assumption about ϵ and δ, then the inversion for several model parameters is unstable, even though the tilt is well-constrained.

To understand the influence of the asymmetry error on the inverted parameters, we repeated the inversion for a wide range of the standard deviations in Δt_{PS} and Δx_{PS} (Figures 8 and 9). Figure 8 shows that for the same errors in the input data, the velocity V_{P0} becomes better constrained for models with larger tilt, whereas for ν the opposite is true. The results for V_{P0} are explained by the much lower sensitivity of this parameter to distortions in the tilt for models with large values of ν (Figure 4b). The standard deviations in the shear-wave

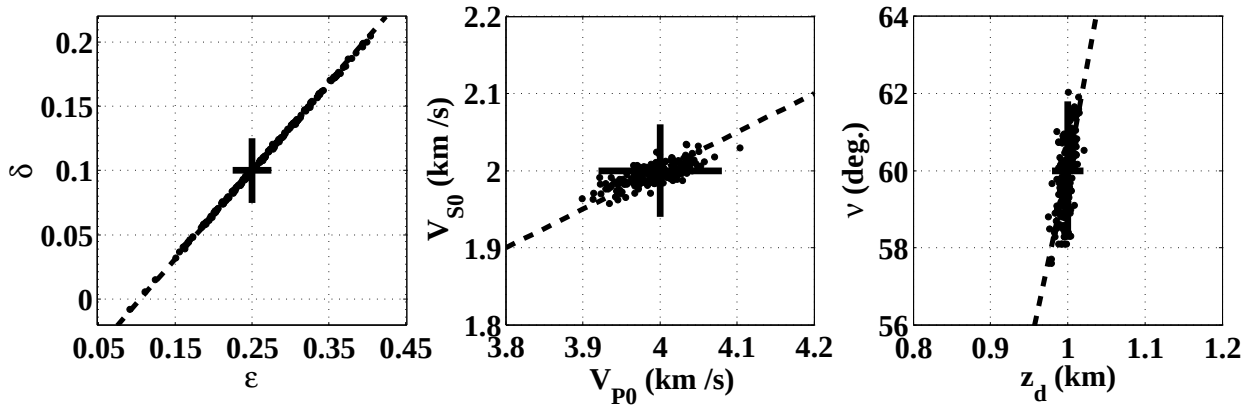

Figure 6. Inverted parameters (dots) of a dipping TTI layer with $\nu = 60°$ obtained from 2-D PP and PS data in the symmetry-axis plane. The correct model parameters are marked by the crosses. The dashed lines on the $[\epsilon, \delta]$, $[V_{P0}, V_{S0}]$, and $[\nu, z_d]$ plots correspond to the correct values of χ, V_{P0}/V_{S0}, and $\sin\nu/z_d$, respectively. The input data were contaminated by Gaussian noise with the standard deviations of 2% for the NMO velocities, 0.5% for the zero-offset traveltimes, 1% for the time slopes, and 2% for the PS-wave asymmetry attributes.

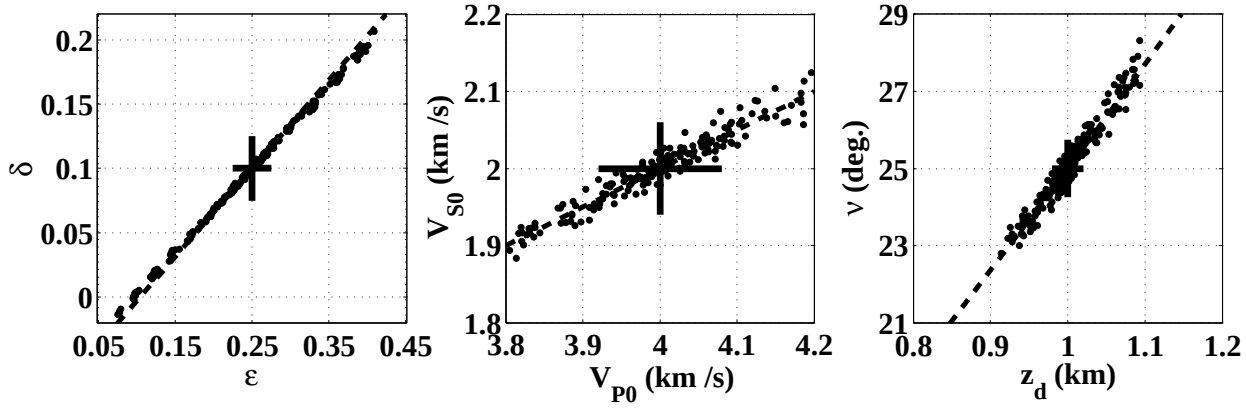

Figure 7. Inversion results for a model with the same parameters as those in Figure 6 except for the tilt $\nu = 25°$. The standard deviations in the asymmetry attributes are increased to 6%; the deviations in the NMO velocities (2%), zero-offset traveltimes (0.5%), and slopes (1%) remain the same.

velocity V_{S0} and the distance z_d are close to those for V_{P0}.

Overall, the tilt remains well resolved for models with $\nu > 10°$ and errors in the asymmetry attributes of up to at least 15% (Figure 8b). The accuracy in the parameters V_{P0}, V_{S0}, and z_d, however, is acceptable only for large tilts over 40° (Figure 8a). For moderate values of ν between 25° and 40°, V_{P0}, V_{S0}, and z_d can be constrained using good-quality converted-wave data that produce small errors in the asymmetry attributes. If the tilt is smaller than 25°, the moveout asymmetry is weak, and the large uncertainty in Δt_{PS} and Δx_{PS} should make the estimates of V_{P0}, V_{S0}, and z_d highly inaccurate.

The standard deviations in the parameters ϵ and δ (Figure 9) show a pattern similar to that for the tilt (Figure 8b). For the same level of the asymmetry errors, both ϵ and δ are better resolved for smaller values of ν. The error curves in Figures 9a and 9b have almost the same shape for all ν because the parameter χ, which is well-constrained by the data, is close to a linear combination of ϵ and δ. However, since ϵ does not directly contribute to the vector of input data, its standard deviation is about 50% larger (on average) than the deviation in δ. Given the likely increase in the asymmetry errors for smaller tilts, the errors in ϵ and δ are expected to be flat for a wide range of moderate and large tilts.

If wide-azimuth PP and PS data are available, we can design a similar inversion algorithm by combining the NMO ellipses, zero-offset traveltimes, and time slopes of the pure modes with the 3D asymmetry attributes of the PSV-wave. Linearization of equa-

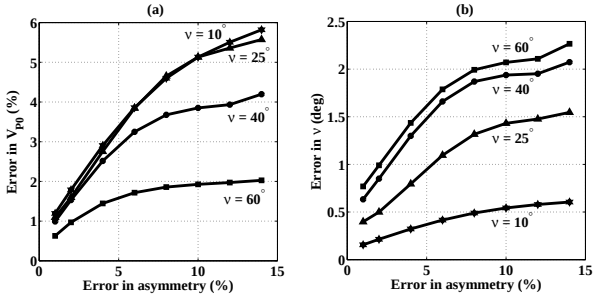

Figure 8. Error (the standard deviation) in the velocity V_{P0} (a) and the tilt ν (b) as a function of the standard deviation in the asymmetry attributes. The tilts are 10° (the line with stars), 25° (triangles), 40° (circles), and 60° (squares). The parameters V_{P0}, V_{S0}, ϵ, δ, and z_d and the standard deviations in the NMO velocities, zero-offset times, and time slopes are the same as those in Figure 6.

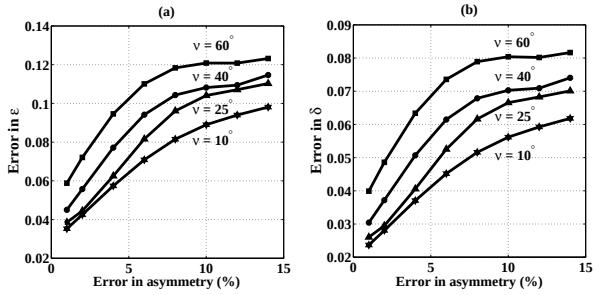

Figure 9. Same as Figure 8, but for the parameters ϵ (a) and δ (b).

tions (A26) and (B8) for small tilts ν shows, however, that the azimuthal variation of the asymmetry attributes can be predicted from their dip components ($\alpha = 0$):

$$\Delta t_{PS}(\alpha) = \Delta t_{PS}(0)\,\cos\alpha, \tag{19}$$

$$\Delta x_{PS}(\alpha) = \Delta x_{PS}(0)\,\cos\alpha. \tag{20}$$

Also, the magnitude of the asymmetry attributes decreases away from the dip direction and goes to zero in the $[x_2, x_3]$-plane. The relatively weak moveout asymmetry for intermediate azimuths means that including the azimuthal variation of Δt_{PS} and Δx_{PS} may not increase the signal-to-noise ratio. A better option for enhancing the signal may be to stack the dip components of the asymmetry attributes for adjacent CMP locations under the assumption of weak lateral heterogeneity. As discussed above [see Figure 3], the pure-mode attributes for small and moderate tilts are too sensitive to noise to help in constraining the model parameters.

For large tilts ($\nu > 40°$), the azimuthal variation of the moveout attributes becomes more complicated and cannot be described by equations (19) and (20). Numerical examples (not shown here) indicate that if $\nu > 40°$, the factors $\Delta t_{PS}(\alpha)$ and $\Delta x_{PS}(\alpha)$ measured in wide-azimuth surveys provide useful constraints on the model parameters. The asymmetry attributes, however, are redundant for large tilts because the inversion can be carried out using wide-azimuth PP and SS data alone (Grechka et al., 2002).

4 DISCUSSION AND CONCLUSIONS

The modified PP+PS=SS method introduced in Part I (Dewangan and Tsvankin, 2003) is applied here to the inversion of multicomponent (PP and PS) data acquired over a dipping TTI layer with the symmetry axis orthogonal to the layer's bottom. As was the case in Part I, the moveout asymmetry attributes of the PSV-wave play a crucial role in the parameter-estimation procedure.

To analyze the moveout asymmetry in the vertical plane that contains the symmetry axis (the symmetry-axis plane), we developed the weak-anisotropy, small-offset approximation for the time (Δt_{PS}) and offset (Δx_{PS}) asymmetry factors. Although the anisotropy has a strong influence on both Δt_{PS} and Δx_{PS} even at small offsets, the leading terms in offset depend just on the moveout parameters of the pure (PP and SS) reflection modes. Therefore, independent information for the inversion procedure is contained only in the higher-order terms that become significant when the offset-to-depth ratio for the PS-waves approaches two.

It should be emphasized that 2D moveout inversion of pure-mode (PP and SS) data in the symmetry-axis plane is nonunique, and even 3D inversion breaks down for small and moderate tilts ν of the symmetry axis. The addition of the PS-wave asymmetry attributes to the NMO velocities, zero-offset traveltimes, and reflection slopes of the recorded PP-waves and the constructed SS-waves can help to invert 2D data in the symmetry-axis plane without *a priori* information. The inversion algorithm is designed as a two-stage procedure, with the factors Δt_{PS} and Δx_{PS} computed only for the family of plausible models which fit the pure-mode data.

To predict the stability of the inversion for a given TTI model, we introduce the "quality factor" (Q) that quantifies the contribution of the cubic and higher-order terms in offset for the time asymmetry Δt_{PS}. Relatively small values of Q ($Q < 1$), which may be caused by a limited offset range of the acquired PP and PS data, typically indicate that the estimated parameters are highly sensitive to noise.

Application of the algorithm to noise-contaminated input data shows that the tilt ν of the symmetry axis is well resolved even when the model approaches VTI ($\nu = 0°$). The accuracy in the symmetry-direction velocities V_{P0} and V_{S0} and the distance z_d from the CMP to the reflector is sufficient only if the symmetry axis deviates by at least 40° from the vertical. For moderate tilts $25° < \nu < 40°$, however, the inversion for V_{P0}, V_{S0}, and z_d is possible only if the errors in the

asymmetry attributes are relatively small. The resolution in the anisotropic parameters ϵ and δ is flat over a wide range of moderate and large tilts, with δ constrained much tighter than is ϵ. For quasi-VTI models with $\nu < 15 - 20^\circ$, the magnitude of the asymmetry attributes is insufficient for reliable estimation of all model parameters, except for the tilt itself.

On the whole, the 2-D inversion in the symmetry-axis plane gives acceptable results if the tilt exceeds 40° and, for high-quality input PS data, for the range of moderate tilts $25^\circ < \nu < 40^\circ$. Still, the accuracy of the inverted parameter ϵ is marginal even for large values of ν (i.e., for steep dips). Note that the inversion for $\nu > 40^\circ$ can be accomplished even without the asymmetry information but it requires wide-azimuth PP and PS (or PP and SS) data (Grechka et al., 2002). The addition of wide-azimuth data (including the asymmetry attributes), however, does not help in the parameter estimation for moderate tilts.

The inversion algorithm developed here makes it possible to build TTI velocity models in depth from multicomponent reflection data without *a priori* information. Taking tilted transverse isotropy into account is particularly important in the presence of dipping shale layers, which are common in fold-and-thrust belts (such as the Canadian Foothills) and near salt domes. The estimated parameters can be used not only for accurate imaging beneath TTI layers, but also for qualitative lithology discrimination.

In this paper, we restrict ourselves to the anisotropic velocity analysis for a single TTI layer and do not address the issue of parameter estimation for multilayered media. Estimation of the effective asymmetry attributes and inversion for the interval parameters of layered TTI models is the subject of our ongoing research.

5 ACKNOWLEDGMENTS

We are grateful to Vladimir Grechka (Shell) and members of the A(nisotropy)-Team of the Center for Wave Phenomena (CWP), Colorado School of Mines, for helpful discussions and to Ken Larner (CSM) for his careful review of the manuscript. The support for this work was provided by the Consortium Project on Seismic Inverse Methods for Complex Structures at CWP and by the Chemical Sciences, Geosciences and Biosciences Division, Office of Basic Energy Sciences, U.S. Department of Energy.

6 REFERENCES

Dewangan, P., and Tsvankin, I., 2003, Application of PS-wave moveout asymmetry in parameter estimation for tilted TI media – Part I: Horizontal TTI layer: CWP Research Report (CWP–465P).

Grechka, V., and Dewangan, P., 2003, Generation and processing of pseudo shear-wave data: Theory and case study: Geophysics, **68**, 1807–1816.

Grechka, V., and Tsvankin, I., 1999, 3-D moveout inversion in azimuthally anisotropic media with lateral velocity variation: Theory and a case study: Geophysics, **64**, 1202–1218.

Grechka, V., and Tsvankin, I., 2000, Inversion of azimuthally dependent NMO velocity in transversely isotropic media with a tilted axis of symmetry: Geophysics, **65**, 232–246.

Grechka, V., and Tsvankin, I., 2002, PP+PS=SS: Geophysics, **67**, 1961–1971.

Grechka, V., Pech, A., Tsvankin, I., and Han, B., 2001, Velocity analysis for tilted transversely isotropic media: A physical-modeling example: Geophysics, **66**, 904–910.

Grechka, V., Pech, A., and Tsvankin, I., 2002, Multicomponent stacking-velocity tomography for transversely isotropic media: Geophysics, **67**, 1564–1574.

Isaac, J. H., and Lawton, D. C., 1999, Image mispositioning due to dipping TI media: A physical seismic modeling study: Geophysics, **64**, 1230–1238.

Lawton, D. C., Issac, J. H., Vestrum, R. W., and Leslie, J. M., 2001, Slip-sliding away - some practical implication of seismic velocity anisotropy on depth imaging: The Leading Edge, **20**, 70–73.

Thomsen, L., 1986, Weak elastic anisotropy: Geophysics, **51**, 1954–1966.

Tsvankin, I., 1995, Normal moveout from dipping reflectors in anisotropic media: Geophysics, **60**, 268–284.

Tsvankin, I., 2001, Seismic signatures and analysis of reflection data in anisotropic media: Elsevier Science Publ. Co., Inc.

Tsvankin, I., and Grechka, V., 2000, Dip moveout of converted waves and parameter estimation in transversely isotropic media: Geophys. Prosp., **48**, 257–292.

Tsvankin, I., and Grechka, V., 2002, 3D description and inversion of reflection moveout of PS-waves in anisotropic media: Geophys. Prosp., **50**, 301–316.

Vestrum, R. W., Lawton, D. C., and Schmid, R., 1999, Imaging structures below dipping TI media: Geophysics, **64**, 1239–1246.

APPENDIX A: APPROXIMATE TIME ASYMMETRY FACTOR FOR THE PSV-WAVE

To derive explicit expressions for the time and offset asymmetry factors in a TTI layer, we use the exact parametric representation of converted-wave moveout developed in Tsvankin (2001, Chapter 5) and Tsvankin and Grechka (2002). The PS-wave reflection traveltime in a homogeneous layer above a plane dipping reflector can be found in the following form:

$$t_{PS} \equiv t_P + t_S = z_r \left(q_P - p_{1P}\, q_{,1P} - p_{2P}\, q_{,2P} + q_S - p_{1S}\, q_{,1S} - p_{2S}\, q_{,2S}\right), \tag{A1}$$

where t_P and t_S are the traveltimes along the P- and S-legs, respectively, z_r is the depth of the conversion point at the reflector, p_1 and p_2 are the horizontal components of the slowness vector (the subscripts "P" and "S" indicate the wave type), $q \equiv p_3$ is the vertical slowness, and $q_{,i} \equiv \partial q/\partial p_i$ $(i = 1, 2)$. According to the convention in Grechka and Tsvankin (2000) and Paper I, the x_3-axis points down, and both legs of the PS ray represent upgoing waves (i.e., the slownesses are computed for group-velocity vectors that point toward the earth's surface). The depth of the conversion point can be represented in terms of the vertical distance $z_{\rm CMP}$ from the common midpoint (CMP) to the reflector:

$$z_r = \frac{z_{\rm CMP}}{1 + \Delta z}, \tag{A2}$$

$$\Delta z = \frac{\tan\phi}{2}\left[(q_{,1P} + q_{,1S})\zeta_1 + (q_{,2P} + q_{,2S})\zeta_2\right]. \tag{A3}$$

Here $\{\zeta_1, \zeta_2\}$ is a horizontal unit vector in the updip direction and ϕ is the reflector dip.

The source-receiver offset x_{PS} of the PS-wave and the azimuth α of the source-receiver line with respect to the x_1-axis can be written as

$$x_{PS} = |\boldsymbol{x}_{PS}| = \sqrt{x_1^2 + x_2^2}, \tag{A4}$$

$$\alpha = \tan^{-1}\left(\frac{x_2}{x_1}\right), \tag{A5}$$

where x_1 and x_2 are the components of the source-receiver vector $\boldsymbol{x}_{PS}$:

$$x_1 = z_r\left(q_{,1P} - q_{,1S}\right), \tag{A6}$$

$$x_2 = z_r\left(q_{,2P} - q_{,2S}\right). \tag{A7}$$

A detailed derivation of equations (A1)–(A7) can be found in Tsvankin (2001, Appendix 5E).

For a weakly anisotropic TTI layer ($|\epsilon| \ll 1$ and $|\delta| \ll 1$), the asymmetry factor Δt_{PS} obtained from the PP+PS=SS method [equations (1) and (2)] can be linearized in the anisotropic coefficients ϵ and δ under the additional assumption of small offset x_{PS}. Here, we consider a TTI layer with the tilt of the symmetry axis equal to the reflector dip (Figure A1). Since the PP+PS=SS method operates with the PP and PS arrivals that have the same reflection point, the projection of the slowness vector onto the reflector is identical (by absolute value) for all reflected waves according to Snell's law.

Using simple trigonometric relationships, the slowness components for the incident and reflected P-waves can be written as

$$p_{\rm i1} = p_{\rm int1}\cos\nu + q^{\rm VTI}\sin\nu, \tag{A8}$$

$$p_{\rm r1} = -p_{\rm int1}\cos\nu + q^{\rm VTI}\sin\nu, \tag{A9}$$

$$p_{\rm i2} = p_{\rm int2} = -p_{\rm r2}, \tag{A10}$$

where $p_{\rm int1}$ and $p_{\rm int2}$ are the slowness components of the incident and reflected waves along the interface in the dip and strike directions, respectively, $q^{\rm VTI}$ is the slowness component in the symmetry-axis direction, $p_{\rm i1}$ and $p_{\rm r1}$ are the horizontal slownesses the incidence and the reflected waves in the symmetry-axis (dip) plane (Figure A1), and $p_{\rm i2}$ and $p_{\rm r2}$ are the slowness components of the incidence and reflected waves in the strike direction. The above relationships between the slownesses remain valid for the S-wave with the same reflection point.

In the weak-anisotropy approximation, $q^{\rm VTI}$ can be expressed for P-waves in terms of $p_{\rm int1}$ and $p_{\rm int2}$ using the VTI equations (Tsvankin and Grechka, 2000):

$$q^{\rm VTI} = q_{P0}\left\{1 - \frac{\left(p_{\rm int1}^2 + p_{\rm int2}^2\right)}{q_{P0}^2}\left[\delta + (\epsilon - \delta)\left(p_{\rm int1}^2 + p_{\rm int2}^2\right)V_{P0}^2\right]\right\}, \tag{A11}$$

$$q_{P0} = \sqrt{\frac{1}{V_{P0}^2} - \left(p_{\rm int1}^2 + p_{\rm int2}^2\right)}. \tag{A12}$$

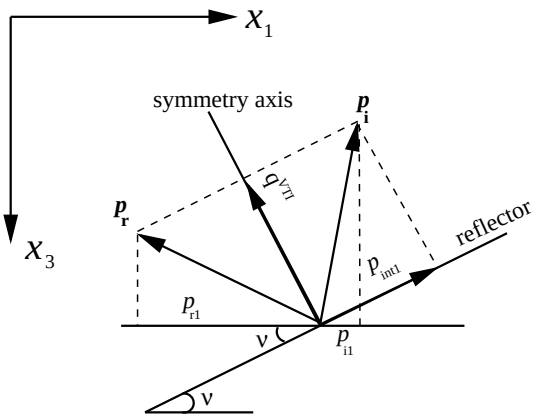

Figure A1. Geometrical relationships between the slowness components of the incidence and reflected P-wave in the dip plane of a TTI layer. The symmetry axis is orthogonal to the dipping interface. $p_{\rm i}$ and $p_{\rm f}$ are the in-plane slowness vectors of the incident and reflected waves, respectively; $p_{\rm i1}$ and $p_{\rm r1}$ are the horizontal slowness components of the incident and reflected waves. $q^{\rm VTI}$ is the slowness along the symmetry axis and $p_{\rm int1}$ is the slowness projection onto the interface in the dip plane.

Substituting the approximate $q^{\rm VTI}$ from equation (A11) into equations (A8) and (A9) and linearizing the resulting expressions for small offset-to-depth ratio ($|p_{\rm int1}\,V_{P0}| \ll 1$, $|p_{\rm int2}\,V_{P0}| \ll 1$), we obtain

$$p_{\rm i1} = \frac{\sin\nu}{V_{P0}} + p_{\rm int1}\cos\nu - \frac{(p_{\rm int1}^2 + p_{\rm int2}^2)\,V_{P0}\sin\nu\,(1+2\delta)}{2}\,, \tag{A13}$$

$$p_{\rm r1} = \frac{\sin\nu}{V_{P0}} - p_{\rm int1}\cos\nu - \frac{(p_{\rm int1}^2 + p_{\rm int2}^2)\,V_{P0}\sin\nu\,(1+2\delta)}{2}\,. \tag{A14}$$

The linearized equation for the vertical slowness components q and their partial derivatives $q_{,i} \equiv \partial q/\partial p_i$ $(i = 1, 2)$ are derived from $p_{\rm i1}$ and $p_{\rm i1}$ following the procedure discussed in Paper I.

If the asymmetry attributes are computed on a line with a fixed azimuth α, the relationship between $p_{\rm int1}$ and $p_{\rm int2}$ can be obtained by linearizing equation (A5):

$$p_{\rm int2} = p_{\rm int1}\,\frac{\tan\alpha}{\cos\nu}\,. \tag{A15}$$

Although this result is derived in the limit of weak anisotropy and small offset, numerical testing shows that is remains valid for arbitrary strength of the anisotropy and the full offset range.

To express the asymmetry attributes as a function of depth beneath the CMP location ($z_{\rm CMP}$), we simplify equations (A2) and (A3) for the depth z_r of the conversion point using the weak-anisotropy, small-offset approximation:

$$z_r = z_{\rm CMP}\,[\cos^2\nu - (1+4\delta)\,p_{\rm int1}^2\,V_{P0}^2\,\sin^2\nu]\,. \tag{A16}$$

The contribution of the P-leg to the time asymmetry can be obtained by substituting equation (A1) into equation (1). We use equations (A13) and (A14) to find the partial derivatives of the vertical slownesses needed in equation (A1), which yields the traveltime as a function of the slowness components $p_{\rm int1}$ and $p_{\rm int2}$ along the interface. Equation (A15) then helps to obtain the time asymmetry factor on a line with the azimuth α. After further linearization in ϵ, δ, and the combinations $|p_{\rm int1}\,V_{P0}|$ and $|p_{\rm int2}\,V_{P0}|$ using symbolic software Mathematica, we find

$$\Delta t_P = 2\,z_{\rm CMP}\,p_{\rm int1}\sin\nu\left[1 + 2\delta + p_{\rm int1}^2\,V_{P0}^2\,(1+4\epsilon)\,\left(1 + \frac{\tan^2\alpha}{\cos^2\nu}\right)\right]\,. \tag{A17}$$

The approximate time asymmetry of the P-leg in equation (A17) is expressed through the slowness $p_{\rm int1}$ that cannot be estimated directly from surface reflection data. It is more practical to represent the asymmetry through the offset x_{PP} of the reflected PP-wave. Substituting the derivatives of the vertical P-wave slowness q_P into equations (A6) and (A7) and evaluating the result for the slownesses given by equation (A13) and (A14), we obtain the PP-wave offset (x_{PP}) from equation (A4):

$$x_{PP} = p_{\rm int1}\,V_{P0}\,z_{\rm CMP}\,\sec\alpha\,\left[2 + 4\delta + p_{\rm int1}^2\,V_{P0}^2\,(1 - 4\delta + 8\epsilon)\,\left(1 + \frac{\tan^2\alpha}{\cos^2\nu}\right)\right]\,. \tag{A18}$$

Equations (A17) and (A18) cannot be used in the strike direction ($\alpha = 90^\circ$) where $p_{\rm int1} = 0$. To remove this ambiguity, we replace $p_{\rm int1}$ with $p_{\rm int2}$ for $\alpha = 90^\circ$ using equation (A15).

It is convenient to expand Δt_P in a Taylor series in x_{PP} around zero offset:

$$\Delta t_P = \frac{\partial \Delta t_P}{\partial x_{PP}}\, x_{PP} + \frac{1}{6}\,\frac{\partial^3 \Delta t_P}{\partial x_{PP}^3}\, x_{PP}^3 + \ldots \tag{A19}$$

Equation (A19) contains only odd powers of offset because the terms even in x_{PP} do not contribute to the moveout asymmetry. Evaluating the partial derivatives in equation (A19) using the chain rule applied to equations (A17) and (A18), we arrive at

$$\Delta t_P = \frac{\sin\nu\,\cos\alpha}{V_{P0}}\, x_{PP} + \frac{(1-2\delta)\,\sin\nu\,\cos^3\alpha}{8\,V_{P0}\,z_{\rm CMP}^2}\left(1+\frac{\tan^2\alpha}{\cos^2\nu}\right) x_{PP}^3\,. \tag{A20}$$

The linearized contribution of the S-leg to the time asymmetry factor can be found from the P-wave equation (A20) using the general transformation rule valid in the limit of weak anisotropy (Tsvankin, 2001, p. 26):

$V_{P0} \to V_{S0}, \quad \epsilon \to 0, \quad \delta \to \sigma\,;$

$$\sigma \equiv \frac{V_{P0}^2}{V_{S0}^2}\,(\epsilon - \delta)\,.$$

The above substitutions give the following expression for the corresponding S-wave asymmetry component Δt_S:

$$\Delta t_S = \frac{\sin\nu\,\cos\alpha}{V_{S0}}\, x_{SS} + \frac{(1-2\sigma)\,\sin\nu\,\cos^3\alpha}{8\,V_{S0}\,z_{\rm CMP}^2}\left(1+\frac{\tan^2\alpha}{\cos^2\nu}\right) x_{SS}^3\,. \tag{A21}$$

Although the common midpoints for the PP- and SS-waves processed by the PP+PS=SS method are not exactly the same, the difference between the values of $z_{\rm CMP}$ for Δt_P and Δt_S can be ignored if the offsets are sufficiently small. Because of the typically large velocity ratios V_{P0}/V_{S0}, the offsets of the constructed SS-wave seldom exceed the reflector depth, so the term x_{SS}^3 in equation (A21) can be neglected.

The total time asymmetry factor of the PS-wave can be found by substituting equations (A20) and (A21) into equation (A1) and taking into account that the contributions of the P-and S-legs should have opposite signs (Paper I):

$$\Delta t_{PS} = \sin\nu\,\cos\alpha\,\left(\frac{x_{PP}}{V_{P0}} - \frac{x_{SS}}{V_{S0}}\right) + \frac{(1-2\delta)\,\sin\nu\cos^3\alpha}{8\,V_{P0}\,z_{CMP}^2}\left(1+\frac{\tan^2\alpha}{\cos^2\nu}\right) x_{PP}^3. \tag{A22}$$

Since the offsets x_{PP} and x_{SS} are related to each other, equation (A22) can be further simplified by expressing x_{PP} through x_{SS}. Applying the transformation P-to-S rule to equation (A18) yields the offset x_{SS} as a function of $p_{\rm int1}$ and azimuth α:

$$x_{SS} = p_{\rm int1}\,V_{S0}\,z_{\rm CMP}\,\sec\alpha\,\left[2+4\sigma+(1-4\sigma)\,p_{\rm int1}^2 V_{S0}^2\left(1+\frac{\tan^2\alpha}{\cos^2\nu}\right)\right]\,. \tag{A23}$$

Expanding x_{PP} in a Taylor series in x_{SS} around zero offset leads to

$$x_{PP} = \frac{\partial x_{PP}}{\partial x_{SS}}\, x_{SS} + \frac{1}{2}\,\frac{\partial^2 x_{PP}}{\partial x_{SS}^2}\, x_{SS}^2 + \frac{1}{6}\,\frac{\partial^3 x_{PP}}{\partial x_{SS}^3}\, x_{SS}^3\,. \tag{A24}$$

The derivatives in equation (A24) can be determined from equations (A18) and (A23), which gives the following expression for the PP-wave offset:

$$x_{PP} = \frac{V_{P0}\,(1+2\delta)}{V_{S0}\,(1+2\sigma)}\, x_{SS} + \frac{(1-4\delta+8\epsilon)\,V_{P0}^3\,\cos^2\alpha}{8\,(1+2\sigma)^3\,V_{S0}^3\,z_{\rm CMP}^2}\left(1+\frac{\tan^2\alpha}{\cos^2\nu}\right) x_{SS}^3\,. \tag{A25}$$

Substituting equation (A25) into equation (A22), we obtain the final expression for the time asymmetry factor in terms of the offset x_{SS}:

$$\Delta t_{PS} = \frac{-2\,(\sigma-\delta)\,\sin\nu\,\cos\alpha}{(1+2\sigma)\,V_{S0}}\, x_{SS} + \frac{(1+4\epsilon)\,V_{P0}^2\,\sin\nu\,\cos^3\alpha}{4\,(1+2\sigma)^3\,V_{S0}^3\,z_{\rm CMP}^2}\left(1+\frac{\tan^2\alpha}{\cos^2\nu}\right) x_{SS}^3\,. \tag{A26}$$

APPENDIX B: APPROXIMATE OFFSET ASYMMETRY FACTOR

Here, we use the approach described in Appendix A to obtain an approximation for the offset asymmetry factor of the PSV-wave in a TTI layer. Using equations (2) and (A6) , the exact parametric equation for the projection of the offset asymmetry vector $\boldsymbol{\Delta x}_{PS}$ onto the x_1-axis can be written as

$$\Delta x_{1_{PS}} \equiv \Delta x_{1P} - \Delta x_{1S} = z_r\,[q_{,P_i} + q_{,P_r} - (q_{,S_i} + q_{,S_r})], \tag{B1}$$

where q is the vertical slowness, $q_{,P_i} \equiv \partial q_P/\partial P_i$, $q_{,P_r} \equiv \partial q_P/\partial P_r$, $q_{,S_i} \equiv \partial q_S/\partial S_i$, and $q_{,S_r} \equiv \partial q_S/\partial S_r$; P_i and P_r the horizontal slownesses for the incident and reflected legs of the P-wave, and S_i and S_r are the same quantities for the S-wave. The slowness vectors are related to each other by Snell's law at the reflection point.

To express the P-wave component of $\Delta x_{1_{PS}}$ as a function of the slowness projection onto the interface in the dip plane ($p_{\rm int1}$), we evaluate the derivatives of the vertical slowness from Appendix A using equations (A13) and (A14):

$$\Delta x_{1_P} = z_r\,(q_{,P_i} + q_{,P_f}) = z_r\,\sec^2\nu\,\tan\nu\,[1 + (2+8\delta)\,p_{\rm int1}^2\,V_{P0}^2 + \cos 2\nu]\,. \tag{B2}$$

It is interesting to note that equation (B2) is independent of $p_{\rm int2}$. The transformation rule gives the corresponding equation for the S-wave:

$$\Delta x_{1_S} = z_r\,\sec^2\nu\,\tan\nu\,[1 + (2+8\sigma)\,p_{\rm int1}^2\,V_{S0}^2 + \cos 2\nu]\,. \tag{B3}$$

Substituting the P- and S-wave asymmetry contributions from equations (B2) and (B3) into equation (B1) yields

$$\Delta x_{1_{PS}} = 2\,z_r\,p_{\rm int1}^2\,\sec^2\nu\,\tan\nu\,[(1+4\delta)\,V_{P0}^2 - (1+4\sigma)\,V_{S0}^2]\,. \tag{B4}$$

Expressing the depth of the reflection point z_r through $z_{\rm CMP}$ using equation (A16), we obtain

$$\Delta x_{1_{PS}} = 2\,z_{\rm CMP}\,p_{\rm int1}^2\,\tan\nu\,[(1+4\delta)\,V_{P0}^2 - (1+4\sigma)\,V_{S0}^2]\,. \tag{B5}$$

To find the factor Δx_{1PS} as a function of the SS-wave offset x_{SS}, we substitute $p_{\rm int1}$ from equation (A23):

$$\Delta x_{1_{PS}} = \frac{\tan\nu}{2\,z_{\rm CMP}}\,\left[\frac{(1+4\delta)\,V_{P0}^2}{(1+4\sigma)\,V_{S0}^2} - 1\right]\,x_{SS}^2\,\cos^2\alpha\,. \tag{B6}$$

The magnitude x_{PS} of the offset asymmetry vector for any azimuth α can be obtained by combining equations (A4) and (A5):

$$\Delta x_{PS} = \frac{\Delta x_{1_{PS}}}{\cos\alpha}\,. \tag{B7}$$

Substituting equation (B6) into equation (B7) yields

$$\Delta x_{PS} = \frac{\tan\nu}{2\,z_{\rm CMP}}\,\left[\frac{(1+4\delta)\,V_{P0}^2}{(1+4\sigma)\,V_{S0}^2} - 1\right]\,x_{SS}^2\,\cos\alpha\,. \tag{B8}$$

In the presence of moveout asymmetry, the minimum traveltime of PS-waves in a CMP gather is not recorded at zero offset. As discussed in Paper I and Tsvankin (2001, Appendix 5B), the offset $x_{\rm min}(\alpha)$ of the traveltime minimum corresponds to the PS ray for which the projections of the slowness vectors for the P- and S-legs onto the CMP line are equal to each other. The dip component of the slowness projection onto the interface can be found in the limit of weak anisotropy, small offset, and small dip as

$$p_{\rm int1}^{\rm min} = \frac{\sin\nu\,\cos^2\alpha}{2}\left(\frac{1}{V_{S0}} - \frac{1}{V_{P0}}\right). \tag{B9}$$

Equation (B9) does not contain any contribution of the anisotropic parameters and coincides with the expression for $p_{\rm int1}^{\rm min}$ in isotropic or VTI media given in Tsvankin (2001, Appendix 5D.2).

Evaluating the derivatives of the vertical slowness (see Appendix A) at $p_{\rm int1}^{\rm min}$ and substituting the result into equations (A6), (A7), and (A4), we find the azimuthally varying offset of the traveltime minimum:

$$x_{\rm min}(\alpha) = \frac{z_{\rm CMP}}{2\,\cos\nu}\,\left[\frac{\sin\nu}{V_{P0}} - \frac{\sin\nu}{V_{S0}}\right]\,[V_{P0}\,(1+2\delta) + V_{S0}\,(1+2\sigma)]\,\cos\alpha\,. \tag{B10}$$